Environmental Science & Technology

pubs.acs.org/est

Article

Dichloramine Hydrolysis in Membrane Desalination Permeate: Mechanistic Insights and Implications for Oxidative Capacity in Potable Reuse Applications

Liang Wu, Sitao Liu, and Haizhou Liu*

Cite This: *Environ. Sci. Technol.* 2024, 58, 13157−13167

Read Online

ACCESS | Metrics & More | Article Recommendations | Supporting Information

ABSTRACT: Dichloramine ($NHCl_2$) naturally exists in reverse osmosis (RO) permeate due to its application as an antifouling chemical in membrane-based potable reuse treatment. This study investigated mechanisms of background $NHCl_2$ hydrolysis associated with the generation of oxidative radical species in RO permeate, established a kinetic model to predict the oxidative capacity, and examined its removal efficiency on trace organic contaminants in potable reuse. Results showed that $NHCl_2$ hydrolysis generated transient peroxynitrite ($ONOO^-$) and subsequently dissociated into hydroxyl radical ($HO^•$). The maximal $HO^•$ exposure was observed at an RO permeate pH of 8.4, higher than that from typical ultraviolet (UV)-based advanced oxidation processes. The $HO^•$ exposure during $NHCl_2$ hydrolysis also peaked at a NH_2Cl-to-$NHCl_2$ molar ratio of 1:1. The oxidative capacity rapidly degraded 1,4-dioxane, carbamazepine, atenolol, and sulfamethoxazole in RO permeate. Furthermore, background elevated carbonate in fresh RO permeate can convert $HO^•$ to carbonate radical ($CO_3^{•-}$). Aeration of the RO permeate removed total carbonate, significantly increased $HO^•$ exposure, and enhanced the degradation kinetics of trace organic contaminants. The kinetic model of $NHCl_2$ hydrolysis predicted well the degradation of contaminants in RO permeate. This study provides new mechanistic insights into $NHCl_2$ hydrolysis that contributes to the oxidative degradation of trace organic contaminants in potable reuse systems.

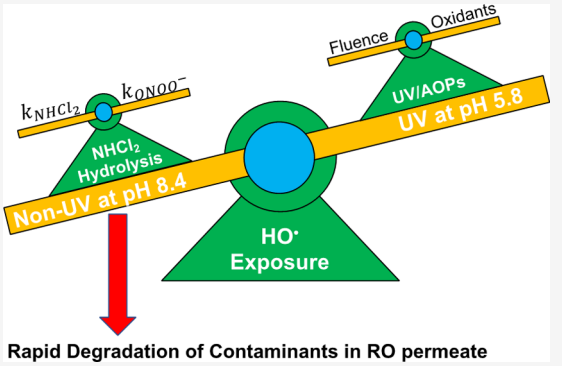

KEYWORDS: *dichloramine, hydrolysis, peroxynitrite, $HO^•$ exposure, 1,4-dioxane, potable reuse*

INTRODUCTION

Growing population, expanding urbanization, and frequent drought severely limit freshwater availability worldwide.[1,2] With the rapid development of advanced water treatment technologies, potable reuse of wastewater effluent becomes invaluable to augment drinking water supplies.[3] Typically, municipal wastewater effluent is fed into a membrane-based water reuse treatment train that sequentially consists of microfiltration (MF), reverse osmosis (RO), and an ultraviolet light-based advanced oxidation process (UV/AOP).[4] Because uncharged and low-molecular-weight trace organic contaminants can pass through RO membranes, and other wastewater effluent-derived organic contaminants can pass through aged RO membranes,[5,6] UV/AOP is employed post-RO to eliminate trace organic contaminants from RO permeate. This process harnesses the generation of reactive radical species from photo-oxidants in a photochemical system with an electrical energy input, facilitating an oxidative degradation of trace organic contaminants.[7,8] Different photo-oxidants including hydrogen peroxide (H_2O_2), persulfate ($S_2O_8^{2-}$), free chlorine (HOCl), and chloramines (NH_2Cl and $NHCl_2$) are applied or proposed.[9−13]

Monochloramine (NH_2Cl), formed by HOCl addition to the typical ammonium ion (NH_4^+)-containing wastewater effluent, is an antifouling chemical widely used in membrane-based potable reuse treatment. Because NH_2Cl passes through RO membranes and subsequently undergoes photolysis,[14−16] the photolysis of NH_2Cl can be harnessed via a UV step to degrade micropollutants in the RO permeate.[11,17,18] Meanwhile, NH_2Cl disproportionates to generate dichloramine ($NHCl_2$) in acidic conditions.[19] The formation of $NHCl_2$ is under a favorable condition in the RO permeate because of its acidic pH (~6) and the absence of NH_4^+ due to the high rejection rate of positively charged ions by the RO membrane (Reaction 1)[20,21]

$$2NH_2Cl + H^+ \rightarrow NHCl_2 + NH_4^+ \quad (R1)$$

Received: May 7, 2024
Revised: June 25, 2024
Accepted: June 25, 2024
Published: July 12, 2024

Prior studies suggest that the decomposition of $NHCl_2$ can lead to an oxidative capacity. For example, the addition of HOCl into NH_4^+ or NH_2Cl was reported to rapidly degrade 1,4-dioxane (1,4-D), an indicator compound regulated for potable reuse in California.[22,23] $NHCl_2$ decomposition also results in the formation of *N*-nitrosodimethylamine (NDMA) when subjected to high radical exposure in the presence of NDMA precursors.[24] Study has investigated $NHCl_2$ decomposition with a focus on NDMA formation and other significant yet unidentified end products through the nitrogen species pathway.[25] In particular, peroxynitrite ($ONOO^-$), a nitrosating agent primarily responsible for NDMA formation in the presence of NDMA precursors, was identified as a critical intermediate during $NHCl_2$ decomposition.[26]

However, the mechanisms of $NHCl_2$ hydrolysis on the production of reactive radical species through oxidative reactions need better understanding. $ONOO^-$ can trigger $HO^\bullet$ generation due to the self-decomposition of its protonated form, peroxynitrous acid (ONOOH).[27,28] Additionally, the oxidative capacity induced by background pre-existing $NHCl_2$ hydrolysis in RO permeate for trace organic degradation under potable reuse conditions has yet to be quantified. Strategies including the upstream removal of precursors (e.g., membrane-based treatments for the removal of large molecules of NDMA precursors) and the post-treatment adjustment of water quality parameters (e.g., increasing pH to destabilize $NHCl_2$) can effectively minimize NDMA formation.[21,29] Moreover, the generated $HO^\bullet$ has been proven effective in degrading NDMA.[30] Hence, the hydrolysis of pre-existing $NHCl_2$ in RO permeate could contribute as a complementary non-UV AOP to conventional UV/AOPs, thereby reducing the electric energy consumption of traditional UV processes.

The pH of RO permeate can significantly impact the oxidative efficiency of $NHCl_2$ hydrolysis in several ways. First, the pH affects the speciation of the chloramines and carbonate, which are photo-oxidants and strong $HO^\bullet$ scavengers, respectively.[31,32] Second, the pH of RO permeate affects the equilibrium between NH_2Cl and $NHCl_2$, which can ultimately change the NH_2Cl-to-$NHCl_2$ molar ratio.[33] In addition, the pH affects the kinetics of chloramine decomposition and the equilibrium of the ONOOH/$ONOO^-$ pair (pK_a = 6.6).[34−37] Therefore, the effects of the RO permeate pH on the $NHCl_2$-initiated oxidative reactions need to be systematically quantified, and the optimal NH_2Cl-to-$NHCl_2$ ratio for $HO^\bullet$ generation needs more exploration.

Furthermore, it is important to examine the effects of total carbonate ($TOTCO_3$) on the oxidative capacity of the $NHCl_2$ hydrolysis because carbonate species can alter radical speciation and contribution.[38] RO desalination is highly pressurized, which increases the solubility of atmosphere carbon dioxide (CO_2) and therefore renders an elevated level of $TOTCO_3$ in RO permeate. This increases the concentrations of dissolved CO_2 and bicarbonate (HCO_3^-) and substantially suppresses the oxidative capacity of $NHCl_2$ hydrolysis.[23] For instance, CO_2 can strongly scavenge $ONOO^-$, preferentially forms selective carbonate radical ($CO_3^{\bullet-}$) via a two-step reaction instead of generating extremely reactive, nonselective $HO^\bullet$.[39] HCO_3^- can also scavenge $HO^\bullet$ to shift the radical speciation toward $CO_3^{\bullet-}$ ($k_{HO^\bullet,HCO_3^-}$ = 8.6 × 10^6 M^{-1} s^{-1}).[40] Therefore, it is crucial to investigate the effects of $TOTCO_3$ on $NHCl_2$ hydrolysis in RO permeate.

Additionally, the efficiency of the $NHCl_2$ hydrolysis on the degradation of indicating trace organic contaminants in potable reuse needs investigation. For example, 1,4-D, a probable human carcinogen,[41] has been widely used as a solvent stabilizer in industry; it passes through RO membranes and exists in RO permeate.[42] Pharmaceuticals including carbamazepine (CBZ), atenolol (ATN), and sulfamethoxazole (SMZ) have been detected in RO permeate, mainly when membrane aged and separation efficiency decreases.[43,44] Consequently, it is important to evaluate the performance of the $NHCl_2$ hydrolysis in potable reuse systems with respect to the removal of these indicating contaminants.[45]

Accordingly, this study aimed to investigate the mechanism of $NHCl_2$ hydrolysis in RO permeate chemical conditions by understanding the reaction pathways leading to the generation of oxidative capacity, quantify the effects of RO permeate chemical parameters (i.e., pH, NH_2Cl-to-$NHCl_2$ ratio, and $TOTCO_3$) on radical yield and speciation, and identify the optimal condition for trace organic removal. 1,4-D, CBZ, ATN, and SMZ were chosen as the indicator organic contaminants to assess the treatment efficiency of the $NHCl_2$ hydrolysis.

MATERIALS AND METHODS

Materials and Reagents. All chemicals were ACS reagent-grade or higher from Fisher Scientific and Sigma-Aldrich. Ultrapure MQ water (>18.2 MΩ·cm, Millipore) was utilized to prepare all solutions except for experiments using RO permeate. The chloramine synthesis followed well-established procedures.[23] Fresh NH_2Cl working solution with negligible ammonia was synthesized by titrating NaOCl to $(NH_4)_2SO_4$ at a nitrogen-to-chlorine molar ratio of 1.2 at pH 8.8 and buffered with 4 mM borate and equilibrated for 2 h before use. Fresh $NHCl_2$ stock solutions were prepared by acidifying the NH_2Cl working solution with 10 M $HClO_4$ to pH 3.5. A 100 mM persulfate stock solution was freshly prepared using $Na_2S_2O_8$. Phosphate buffers to control pHs between 7 and 9 were made using a predetermined combination of NaH_2PO_4 and Na_2HPO_4. Borate buffers to control pH values above 9 consisted of a proper combination of H_3BO_3 and $Na_2B_4O_7$. $ONOO^-$ stock solutions were synthesized by rapidly adding HCl to the mixed solution containing H_2O_2 and $NaNO_2$ with instant quench using NaOH.[46] Details on the preparation of the $ONOO^-$ solutions are provided in Text S1 in the Supporting Information (SI). Other working solutions of photo-oxidants (i.e., H_2O_2, HOCl, and $S_2O_8^{2-}$) were prepared freshly.

Synthetic fresh RO permeate was prepared by combining 1 μg/L trace organic contaminants (specifically, 1,4-D, CBZ, ATN, or SMZ), 3 mg/L $NHCl_2$, and 2 mM $NaHCO_3$ at pH 5.8. The concentrations of these chemical components represent realistic RO permeate conditions. The synthetic aerated RO permeate sample was prepared the same way with the addition of 0.05 mM $NaHCO_3$. These carefully chosen levels of $TOTCO_3$ represent the background carbonate levels in fresh RO permeate and post-treatment after aeration, respectively.

Fresh RO permeate was collected in situ from a full-scale municipal potable reuse facility at Orange County Water District (OCWD) in Fountain Valley, California. Fresh RO permeate was collected from the outlet of the full-scale RO permeate module and preserved in a 4 L amble bottle without headspace. Aerated RO permeate was prepared by purging air

https://doi.org/10.1021/acs.est.4c04547
Environ. Sci. Technol. 2024, 58, 13157−13167

to the fresh RO permeate in a 4 L beaker with constant agitation for 2 h on-site to remove $TOTCO_3$.

Bench-Scale Experiments on $NHCl_2$ Hydrolysis and Oxidative Reactions. Bench-scale $NHCl_2$ hydrolysis experiments were conducted in a 50 mL Petri dish reactor in triplicates at 25 °C. The predetermined buffer volume at the targeted pH and nitrobenzene (NB) were added to the Petri dish reactor. Following that, an appropriate amount of fresh $NHCl_2$ stock solution was added to the reactor to start the reaction, creating an initial solution containing 3 mM $NHCl_2$, 5 μM NB, and 60 mM buffer under constant rapid agitation. The initial $NHCl_2$ concentration of 3 mM was chosen to allow for accurate radical quantification. Samples were withdrawn from the reactor at 0 and 15 s of the hydrolysis reaction for immediate chemical analysis. The reaction time of 15 s was selected based on the rapid kinetics observed in preliminary experiments.

To investigate the effects of pH on $NHCl_2$ hydrolysis, buffers were introduced to the reactor with pHs ranging from 7 to 12. This wide pH range allows for a mechanistic investigation of the reaction system. Solution pH was stable during the experiments. To explore the effects of the NH_2Cl-to-$NHCl_2$ ratio on $NHCl_2$ hydrolysis, varying levels of fresh NH_2Cl stock solutions were added to the reactor in separate experiments to obtain a NH_2Cl-to-$NHCl_2$ molar ratio between 0 and 3, which covers relevant conditions in real-world potable reuse scenarios. Additional experiments to investigate carbonate effects were conducted by adding $NaHCO_3$ to obtain a $TOTCO_3$ level between 0.1 and 20 mM at pH 8.4. HCO_3^- was utilized to simulate scenarios in real-world RO permeate, as the highly pressurized RO process increases the solubility of CO_2 in acidic RO permeate, and it is transformed to HCO_3^- when the RO permeate is neutralized to a higher pH as final treated water. Twenty μM *N*,*N*-dimethylaniline (DMA) was added as the $CO_3^{\bullet-}$ exposure probe, and 5 μM NB was added as the $HO^\bullet$ exposure probe in carbonate experiments. Furthermore, bench-scale $NHCl_2$ hydrolysis experiments were conducted using synthetic RO permeates at a pH of 8.4, employing 0.8 μM NB as a probe compound to quantify the exposure to $HO^\bullet$.

Experiments on $NHCl_2$ Hydrolysis Using RO Permeate at a Potable Reuse Facility. To assess the effectiveness of the proposed $NHCl_2$ hydrolysis as a novel non-UV AOP for degrading trace-level organic contaminants, field experiments were conducted at OCWD using fresh RO permeate from their full-scale municipal potable reuse facility. Fresh RO permeate was collected first. In addition, to evaluate the effects of aeration of RO permeate on oxidative capacity, additional freshly collected RO permeate was bubbled with air at ambient temperature for up to 2 h to degas and produce the aerated RO permeate. The concentrations of pre-existing NH_2Cl and $NHCl_2$, pH, and $TOTCO_3$ in both fresh and aerated RO permeate samples were measured, and the RO permeate was subsequently transferred to a 500 mL reactor. Background $NHCl_2$ was already present in the fresh RO permeate, and additional freshly prepared $NHCl_2$ stock was added to obtain an initial $NHCl_2$ concentration of 3 mg/L in the RO permeate for the field experiment. This targeted level of $NHCl_2$ falls within the typical background concentration found in realistic RO permeate.[5] Additionally, the solution was spiked with 1 μg/L of 1,4-D and 0.8 μM NB. After that, the RO permeate was adjusted to a pH of 8.4 to start hydrolysis reactions, and samples were taken after 15 s of reaction for analysis.

Decomposition of $NHCl_2$ and $ONOO^-$ and UV Photolysis Experiments. Experiments on $NHCl_2$ and $ONOO^-$ decay kinetics were conducted in a 3-mL quartz cuvette reactor at pHs from 7 to 12. Details of the decomposition experiments are provided in Text S2 and Figures S1 and S2. Control UV/AOP experiments with different photo-oxidants (i.e., H_2O_2, HOCl, $S_2O_8^{2-}$, NH_2Cl, $NHCl_2$, NH_2Cl with H_2O_2, and $NHCl_2$ with H_2O_2) were conducted to compare with the oxidative capacity of the $NHCl_2$-initiated non-UV hydrolysis AOP. UV/AOP control experiments were conducted at pH 5.8 (typical RO permeate pH) in a 50-mL Petri dish reactor under constant agitation with a 254 nm low-pressure mercury lamp (Ultra Sum Technologies). The UV fluence of the UV system was determined by atrazine actinometry to confirm the targeted value of 850 mJ/cm^2, which is the typical UV fluence received by RO permeate at the full-scale UV/AOP treatment.[47] Details on the UV/AOP control experiments are provided in Text S3.

Analytical Methods. Each sample taken from the $NHCl_2$ hydrolysis experiments was analyzed for concentrations of NH_2Cl and $NHCl_2$ using the standard *N*,*N*-diethyl-*p*-phenylenediamine (DPD) method.[48] Alkalinity was measured according to the standard titration method.[49] Probe compounds of NB and DMA were quantified by utilizing high-performance liquid chromatography coupled with a diode array detector (HPLC-DAD, Agilent). Trace concentrations of 1,4-D (1 μg/L or less) were determined according to EPA Method 522 by gas chromatography coupled with mass spectrometry (GC-MS, Agilent). Trace concentrations of CBZ, ATN, and SMZ were analyzed by ultrahigh-performance liquid chromatography coupled with high-resolution tandem mass spectrometry (HPLC-HRMS/MS, Q Exactive, Thermo Fisher Scientific). Details of analytical methods for 1,4-D and all indicator compounds are provided in Text S4. The concentration of H_2O_2 was quantified by the titanium oxalate method.[50] Concentration of $S_2O_8^{2-}$ was determined using the KI titration method.[51] The stock solution of $ONOO^-$ was determined via a direct absorbance method at 302 nm.[46]

To determine the cumulative $HO^\bullet$ exposure from $NHCl_2$ hydrolysis and UV/AOP control, NB was used as a selective $HO^\bullet$ probe (details regarding the calculation of cumulative $HO^\bullet$ exposure are provided in Text S5 and Table S1). To quantify the contribution of radicals during $NHCl_2$ hydrolysis, NB and DMA were utilized as probe compounds for $HO^\bullet$ and $CO_3^{\bullet-}$, respectively.[52,53] A competition kinetic method was used for calculating the steady-state concentrations for the eventual calculation of the cumulative exposure of $HO^\bullet$ and $CO_3^{\bullet-}$ (Text S5).

Mathematical Model to Predict the Oxidative Capacity of $NHCl_2$ Hydrolysis. A mathematical model was established to predict the oxidative capacity of the $NHCl_2$ hydrolysis-initiated AOP based on reaction pathways and mechanisms discovered in this study. The optimization of the model was carried out using a training data set composed of experimental data on the hydrolysis of $NHCl_2$ and $ONOO^-$ to fit the $HO^\bullet$ reaction efficiency coefficient α in the model. A comprehensive global fitting procedure was employed to fit the experimentally observed mean values of $HO^\bullet$ exposure to model-predicted outcomes by optimizing the value of an intrinsic model parameter, γ, which is the NH_2Cl effect factor. During the model fitting to correlate the experimentally observed and model-predicted $HO^\bullet$ exposure data, the slope was constrained to be within 1 ± 0.25, the intercept $\leq 2 \times$

https://doi.org/10.1021/acs.est.4c04547
Environ. Sci. Technol. 2024, 58, 13157−13167

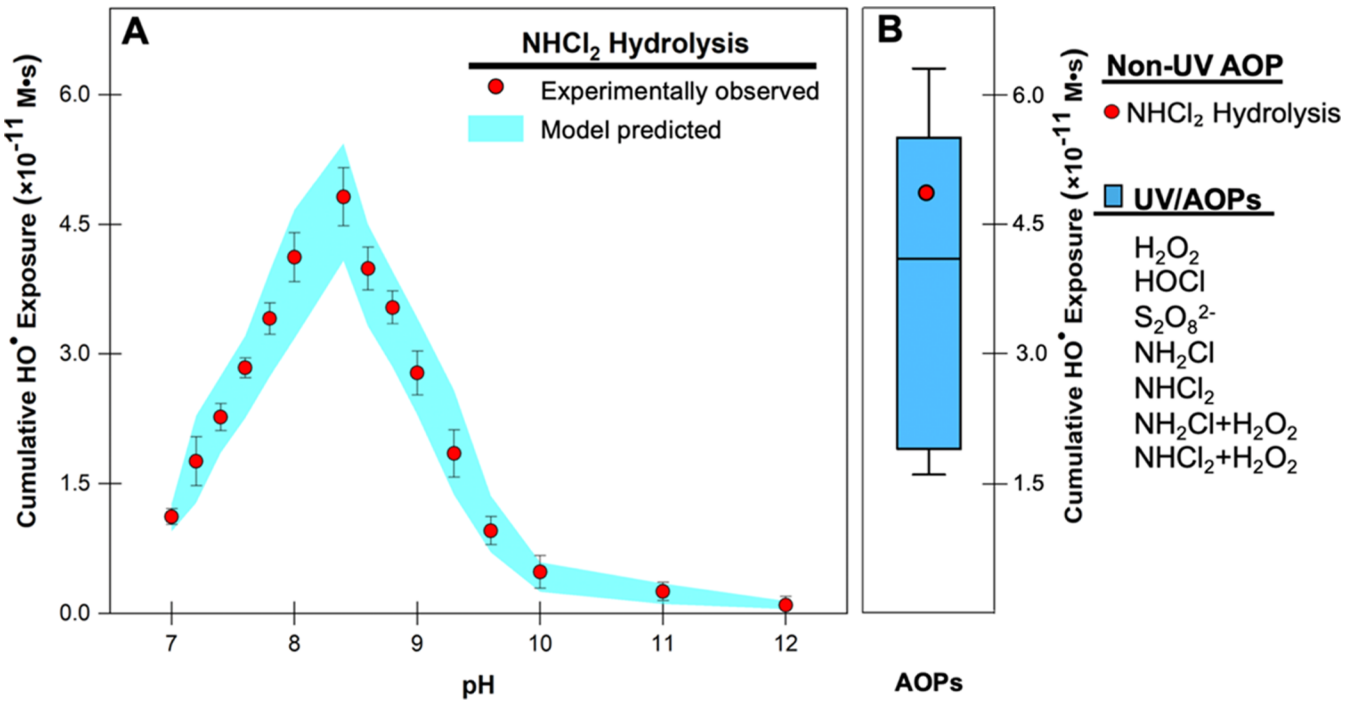

Figure 1. Cumulative hydroxyl radical exposure of non-UV $NHCl_2$ hydrolysis vs traditional UV/AOPs. (A) $NHCl_2$ hydrolysis at pH 7−12. Buffer = 60 mM for all pHs, $[NHCl_2]_0$ = 3 mM, $[NB]_0$ = 5 μM, and reaction time = 15 s. (B) UV photolysis of H_2O_2, HOCl, $S_2O_8^{2-}$, NH_2Cl, and $NHCl_2$ at pH 5.8; in the single-oxidant UV/AOP system: $[oxidant]_0$ = 1 mM; in the combined-oxidant UV/AOP system, $[chloramine]_0$ = 1 mM, $[H_2O_2]_0$ = 2 mM; $[NB]_0$ = 100 μM, UV fluence = 850 mJ/cm^2. The solid line in the box plot is the median value, and the lower and upper box edges are the 25th and 75th percentiles. Whisker bars represent the minimum and maximum values. Details of the HO$^\bullet$ exposure of UV/AOPs are provided in Table S6. Mathematical model fitting represents one standard deviation of the prediction: α = 0.25 ± 0.05, γ = 1 (details of the model fitting are provided in Text S6). The predicted shaded area represents a 68% confidence interval. Error bars represent the standard deviation of experimental triplicates.

Scheme 1. Reaction Scheme for the $NHCl_2$ Hydrolysis System, with Proposed Reaction Pathways for the Generation of Reactive Species Responsible for Micropollutant Degradation[a]

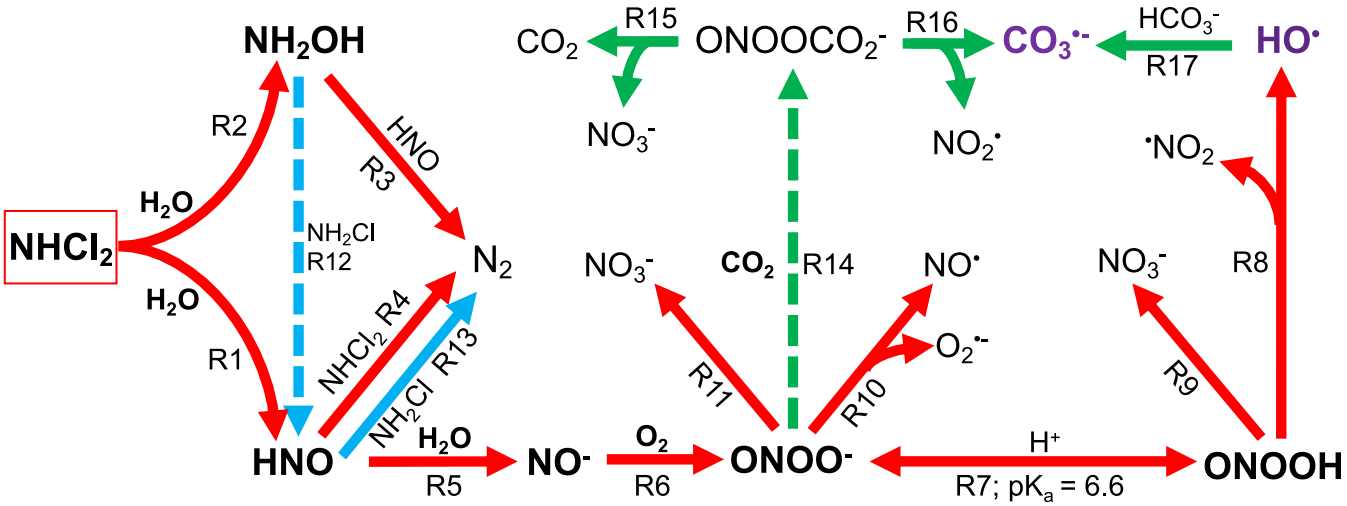

[a]Major reaction pathways (red), generated radicals for micropollutant removal (purple), NH_2Cl-related reactions (blue), and scavenging reactions (green).

10^{-5}, and the $R^2 \geq 0.85$. The detailed model optimization procedure is provided in Text S6. The fully optimized model was tested to predict the removal of trace organic contaminants under both synthetic and RO permeate conditions.

RESULTS AND DISCUSSION

Mechanisms of pH Effects on $NHCl_2$ Hydrolysis and Cumulative HO$^\bullet$ Exposure. The oxidative capacity of the $NHCl_2$ hydrolysis system was examined as a function of the solution pH. The degradation of NB was observed during the $NHCl_2$ hydrolysis within 15 s at pHs ranging from 7 to 12 (Figure 1A). The results demonstrated that HO$^\bullet$ was

https://doi.org/10.1021/acs.est.4c04547
Environ. Sci. Technol. 2024, 58, 13157−13167

generated through the hydrolytic decay of $NHCl_2$ at pH levels where $NHCl_2$ is unstable, consistent with observations from our previous study.[23] In the $NHCl_2$-initiated hydrolysis system, when $NHCl_2$ destabilizes at certain pH levels, it undergoes hydrolytic decay, producing nitroxyl (HNO) and hydroxylamine (NH_2OH) via R1 and R2, respectively (R1 and R2 in Scheme 1; the following reactions all refer to Scheme 1).[26,54] NH_2OH further reacts with HNO to form nitrogen gas (N_2) via R3.[55] HNO reacts with $NHCl_2$ as a side reaction to produce N_2 (R4), but more significantly, HNO deprotonates to form nitric oxide anion (NO^-) via R5, which is further rapidly oxidized by dissolved oxygen in the solution to generate the critical intermediate peroxynitrite ($ONOO^-$; R6; $k = 2.7 \times 10^9\ M^{-1}\ s^{-1}$).[56,57] Upon protonation, $ONOO^-$ becomes peroxynitrous acid (ONOOH; R7; $pK_a = 6.6$).[37] Most importantly, ONOOH directly decays into $HO^\bullet$ and nitrogen dioxide radical ($^\bullet NO_2$) via R8 ($k = 3.5 \times 10^{-1}\ s^{-1}$) or produces NO_3^- as a stable product via R9 ($k = 9.0 \times 10^{-1}\ s^{-1}$).[58] Meanwhile, $ONOO^-$ undergoes self-decomposition into $NO^\bullet$ and $O_2^{\bullet-}$ (R10; $k = 2.3 \times 10^{-2}\ s^{-1}$) or yields nitrate ($NO_3^-$) by R11 ($k = 9.0 \times 10^{-6}\ s^{-1}$).[54,58] The generated $HO^\bullet$ was not scavenged by the maximum 3 mM chloride (Cl^-), which was introduced by the NaOCl solution utilized for NH_2Cl preparation (detailed calculations are provided in Text S5). This is because the first-order reaction rate of the forward reaction ($HO^\bullet + Cl^- \rightarrow ClOH^{\bullet-}$; $k \times [Cl^-] = 1.3 \times 10^7\ s^{-1}$) is much slower than the backward reaction ($ClOH^{\bullet-} \rightarrow HO^\bullet + Cl^-$; $k = 6.1 \times 10^9\ s^{-1}$).[59]

The maximal $HO^\bullet$ exposure peaked at pH 8.4 and decreased either toward a neutral pH of 7 or at higher alkaline pHs up to 12, with suppressing percentages of 77 and 98% (Figure 1A), respectively. $HO^\bullet$ generated from $NHCl_2$ hydrolysis can greatly benefit micropollutant abatement due to its high cumulative exposure within a short time.[22] At the optimal pH of 8.4, the cumulative $HO^\bullet$ exposure within 15 s of $NHCl_2$ hydrolysis was 4.8×10^{-11} M·s, a level that stands out as a very high value when compared with the $HO^\bullet$ exposure levels generated by existing UV/AOPs commonly utilized or suggested for implementation in potable reuse systems (Figure 1B). $HO^\bullet$ exposure from UV/AOPs is between 1.6 and 6.3×10^{-11} M·s. The fact that the optimal oxidative capacity of the $NHCl_2$ hydrolysis is at the higher end of UV irradiation-based AOPs for water reuse is very promising, suggesting an alternative non-UV-based AOP with significantly less energy footprint due to the omission of UV lamps and photon energy.

Prior literature proposed a two-step decay pathway that leads to $HO^\bullet$ generation, via first $NHCl_2$ undergoing a hydrolytic decay to form $ONOO^-$ (Reactions R1−R6), and subsequently the generated $ONOO^-$ yields $HO^\bullet$ (R7-R8).[22] The decay of $NHCl_2$ and $ONOO^-$ was quantified through the decomposition experiments and data showed that the $NHCl_2$ hydrolysis rate increased by more than 1 order of magnitude when the solution pH increased from 7 to 12, increasing from 1.4×10^{-2} to $1.9 \times 10^{-1}\ s^{-1}$ (Figure 2). This is because $NHCl_2$ hydrolysis favors alkaline conditions and becomes unstable when the pH is above neutral.[60] In contrast, the decomposition rate of $ONOO^-$ increased by nearly 2 orders of magnitude when the pH decreased from 12 to 7. $ONOO^-$ remians stable as an anion at alkaline pH levels. However, as the pH decreases and protonation occurs, $ONOO^-$ rapidly decomposes into $HO^\bullet$ and $^\bullet NO_2$ (R7−R8). The opposite trends in $NHCl_2$ and $ONOO^-$ decay rates (Figure 2) created a combined effect on

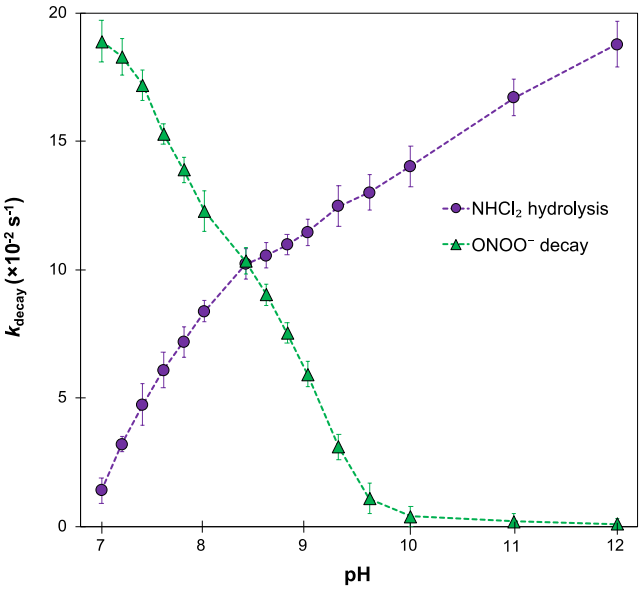

Figure 2. Experimentally observed *pseudo*-first-order rates of $NHCl_2$ hydrolysis and $ONOO^-$ decay at different pHs. Buffer = 60 mM at all pHs, $[NHCl_2]_0 = 42\ \mu M$, $[ONOO^-]_0 = 850\ \mu M$, and reaction time = 15 s. Error bars represent the standard deviation of experimental triplicates.

$HO^\bullet$ formation that peaked at an intermediate pH level between 7 and 12 (i.e., at pH 8.4 as observed in Figure 1A).

Mechanisms of NH_2Cl-to-$NHCl_2$ Molar Ratio Effects on $NHCl_2$ Hydrolysis and $HO^\bullet$ Exposure. The NH_2Cl-to-$NHCl_2$ molar ratio greatly affected the oxidative capacity of the $NHCl_2$ hydrolysis system (Figure 3A). The $HO^\bullet$ exposure was the highest at a NH_2Cl-to-$NHCl_2$ molar ratio of 1 and declined when the NH_2Cl-to-$NHCl_2$ molar ratio deviated from 1. The $HO^\bullet$ exposure was suppressed by 19 and 47% when shifting the NH_2Cl-to-$NHCl_2$ molar ratio from 1 to 0 and 3, respectively. These trends of molar ratio effects resulted from two competing effects of NH_2Cl on $HO^\bullet$ exposure during $NHCl_2$ hydrolysis. When NH_2Cl is introduced to the $NHCl_2$-initiated AOP system, the generated NH_2OH reacts with NH_2Cl to form HNO (R12 in Scheme 1).[61] The formation of HNO resulted in higher $HO^\bullet$ exposure, as HNO is the primary precursor for the subsequent generation of $ONOO^-$/ONOOH, leading to $HO^\bullet$ production (R5−R8). However, as the concentration of NH_2Cl further increases, it also scavenges HNO to produce N_2 (R13).[56] As the NH_2Cl-to-$NHCl_2$ molar ratio increases beyond the optimal level, R13 becomes more dominant than R12, consequently leading to a more substantial scavenging effect rather than a promoting effect on $HO^\bullet$ exposure. The trade-off effects led to an optimal NH_2Cl-to-$NHCl_2$ molar ratio at 1 during $NHCl_2$ hydrolysis on $HO^\bullet$ exposure (Figure 3A).

At the optimal NH_2Cl-to-$NHCl_2$ molar ratio of 1, the highest $HO^\bullet$ exposure of 5.9×10^{-11} M·s was observed at pH 8.4, consistent with the pH effects in the absence of NH_2Cl (Figure 1A). It showed an approximately 23% enhancement compared with the system without NH_2Cl across all pHs (Figures 3B vs 1A). The results suggested that NH_2Cl promoted $HO^\bullet$ exposure across a wide solution pH during $NHCl_2$ hydrolysis.

Mechanisms of Carbonate Effects on $NHCl_2$ Hydrolysis and Radical Speciation. Fresh RO permeate is elevated in dissolved CO_2 and therefore $TOTCO_3$ due to enhanced

https://doi.org/10.1021/acs.est.4c04547
Environ. Sci. Technol. 2024, 58, 13157−13167

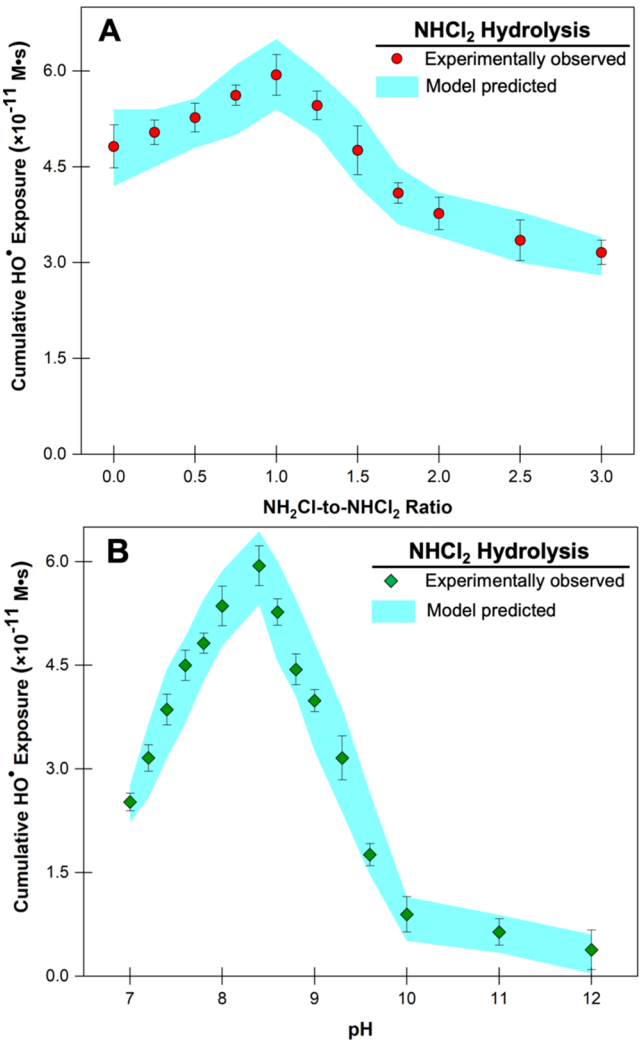

Figure 3. Cumulative hydroxyl radical exposure via $NHCl_2$ hydrolysis. Buffer = 60 mM for all pHs, $[NHCl_2]_0$ = 3 mM, $[NB]_0$ = 5 μM, and reaction time = 15 s. (A) NH_2Cl-to-$NHCl_2$ molar ratio effects at pH 8.4; (B) pH effects at the NH_2Cl-to-$NHCl_2$ molar ratio of 1. Mathematical model fitting represents one standard deviation of the prediction: α = 0.25 ± 0.05, γ = 1 (details of the model fitting are provided in Text S6). The predicted shaded area represents a 68% confidence interval. Error bars represent the standard deviation of experimental triplicates.

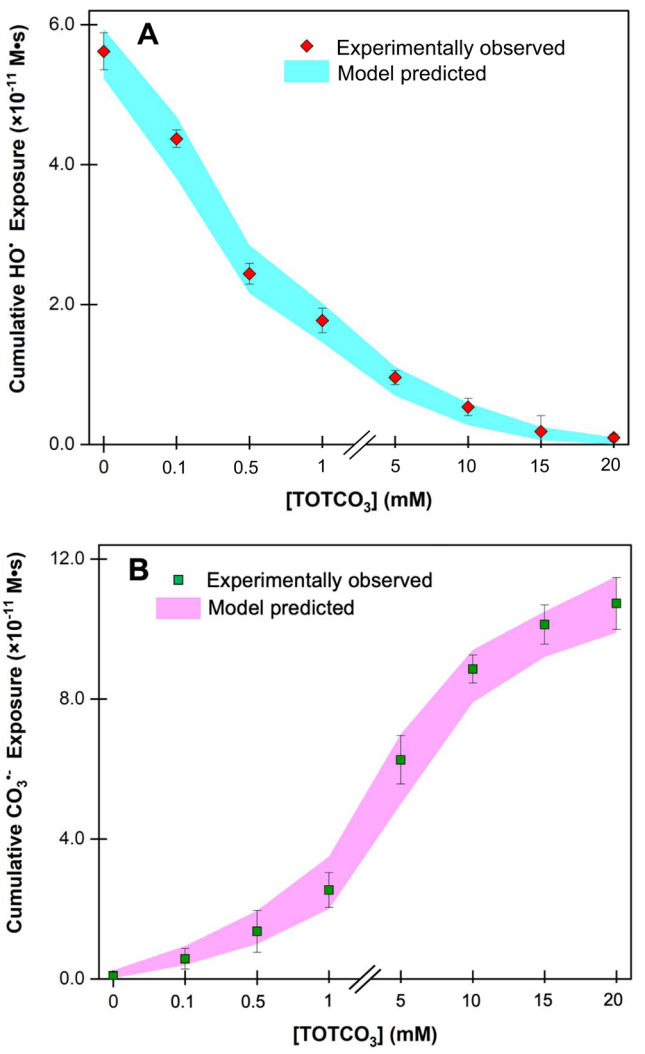

Figure 4. Cumulative radical exposure during $NHCl_2$ hydrolysis under pH 8.4 at varying $TOTCO_3$ concentrations. (A) Cumulative $HO^•$ exposure; (B) cumulative $CO_3^{•-}$ exposure. $[NHCl_2]_0$ = 3 mM, $[NB]_0$ = 5 μM, $[DMA]_0$ = 20 μM, and reaction time = 15 s. Mathematical model fitting represents one standard deviation of the prediction: α = 0.25 ± 0.05, γ = 1 (details of the model fitting are provided in Text S6). The predicted shaded area represents a 68% confidence interval. Error bars represent the standard deviation of experimental triplicates.

dissolution of the gas from pressurized air during RO operation and the fact that RO permeate is acidic. Harnessing the oxidative capacity of the $NHCl_2$ hydrolysis to its maximum needs to consider the $TOTCO_3$ effects. At acidic pHs, $ONOO^-$ is scavenged by the dissolved CO_2 to form $ONOOCO_2^-$ (R14 in Scheme 1; $k = 2.9 \times 10^4$ M^{-1} s^{-1}), which then self-decomposes into CO_2 and NO_3^- (R15) or decays into $CO_3^{•-}$ and $NO_2^•$ (R16).[39,62] Additionally, at neutral-to-alkaline pHs, $HO^•$ is further converted to $CO_3^{•-}$ by HCO_3^- (R17; $k = 8.6 \times 10^6$ M^{-1} s^{-1}).[40] Therefore, the $HO^•$ exposure is suppressed and converted to $CO_3^{•-}$ exposure in the presence of $TOTCO_3$.

Experimental results showed that the cumulative $HO^•$ exposure was reduced by 30% in the presence of 0.1 mM $TOTCO_3$, further reduced by 70% when the $TOTCO_3$ level reached 1 mM, and suppressed to a negligible level in the presence of 20 mM $TOTCO_3$ (Figure 4A). The scavenging of $HO^•$ was accompanied by an increase in the level of $CO_3^{•-}$ exposure. The $CO_3^{•-}$ exposure was enhanced by nearly 19-fold when the $TOTCO_3$ was shifted from 0.1 to 20 mM (Figure 4B). Because the standard RO process is pressurized and elevates the dissolution of CO_2, the high $TOTCO_3$ levels in fresh RO permeate can compromise the $HO^•$ exposure. Consequently, the $HO^•$-driven oxidative capacity of the $NHCl_2$-based AOP favors a low $TOTCO_3$, which can be achieved by an aeration step to decarbonize the fresh RO permeate in the water reuse facilities.

$NHCl_2$ Hydrolysis AOP in Synthetic RO Permeate Conditions. $NHCl_2$ hydrolysis-based AOP significantly degraded the four relevant trace organic contaminants in the synthetic RO permeate (Figure 5A). Under normal RO operation, the fresh RO permeate contains high levels of $TOTCO_3$ that can be up to 2 mM (details are provided in Text S7). The experimentally observed *pseudo*-first-order degrada-

https://doi.org/10.1021/acs.est.4c04547
Environ. Sci. Technol. 2024, 58, 13157−13167

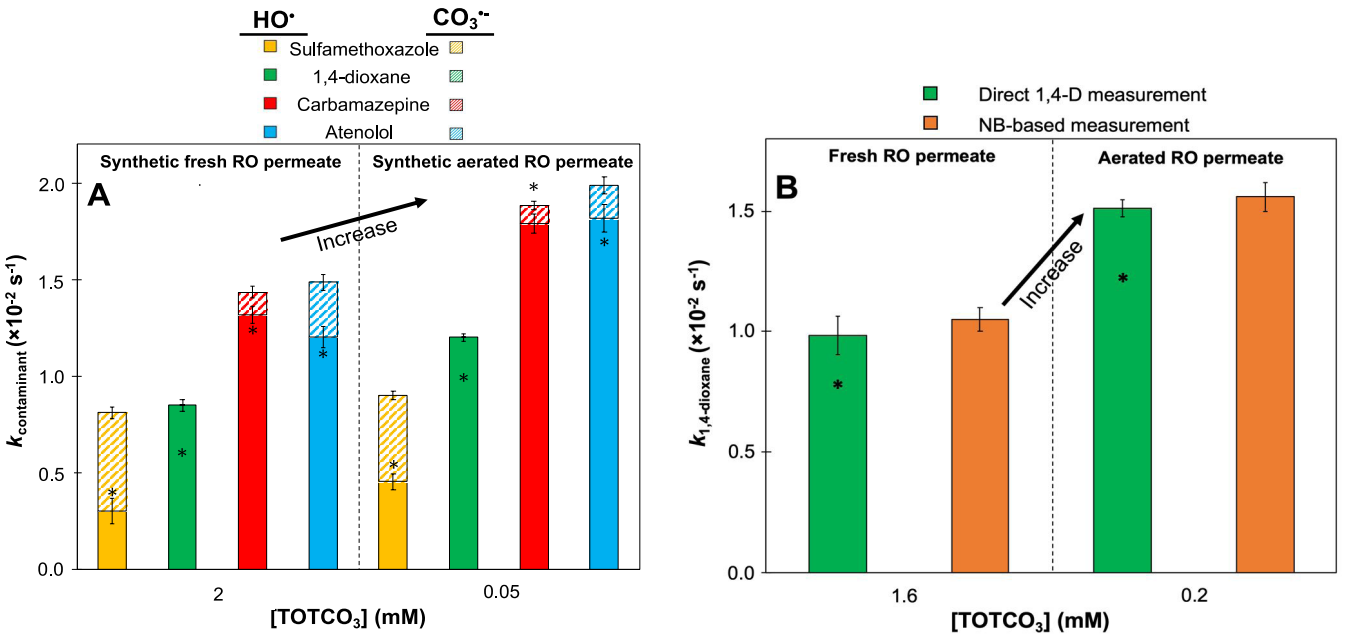

Figure 5. Effects of $TOTCO_3$ on *pseudo*-first-order degradation rates of trace contaminants via $NHCl_2$ hydrolysis at pH 8.4 under synthetic RO permeate vs RO permeate. The sign of "*" represents the predicted *pseudo*-first-order rates of trace contaminants by the mathematical model (details of the model prediction are provided in Text S6). (A) Synthetic fresh RO permeate: $[TOTCO_3]_0$ = 2 mM; synthetic aerated RO permeate: $[TOTCO_3]_0$ = 0.05 mM, buffer = 60 mM, $[NHCl_2]_0$ = 3 mg/L, $[1,4\text{-D}]_0$ = 1 μg/L, $[CBZ]_0$ = 1 μg/L, $[ATN]_0$ = 1 μg/L, $[SMZ]_0$ = 1 μg/L, $[NB]_0$ = 0.8 μM; (B) fresh RO permeate: $[TOTCO_3]_0$ = 1.6 mM; aerated RO permeate: $[TOTCO_3]_0$ = 0.2 mM, $[NHCl_2]_0$ = 3 mg/L, $[NH_2Cl]_0$ = 2.1 mg/L, $[1,4\text{-D}]_0$ = 1 μg/L, $[NB]_0$ = 0.8 μM. Reaction time = 15 s. Error bars represent the standard deviation of the experimental triplicate.

tion rates (denoted as $k_{contaminant}$) of SMZ, 1,4-D, CBA, and ATN were 8.1×10^{-3}, 8.5×10^{-3}, 1.4×10^{-2}, and 1.5×10^{-2} s^{-1}, respectively (left panel in Figure 5A). When the RO permeate undergoes an aeration process to decarbonate, the $TOTCO_3$ level in the RO permeate can be reduced to 0.05 mM (details are provided in Text S7). In this scenario, the experimentally observed degradation rates for all selected compounds were significantly enhanced (by up to 140%) in comparison to the normal RO operation conditions (right panel in Figure 5A). In both scenarios, the contribution of $HO^•$ to the degradation of trace organic contaminants is predominant.

Specifically, when the RO permeate is aerated to decarbonate, the degradation rate of SMZ increased by 11% because the rate constants of SMZ with $HO^•$ and $CO_3^{•-}$ are comparable (rate constants between the four selected contaminants with $HO^•$ and $CO_3^{•-}$ are provided in Table S2).[63,64] 1,4-D degradation rate was enhanced by 42% because it reacts with $HO^•$ but is not reactive with $CO_3^{•-}$.[65,66] Therefore, the 1,4-D degradation favors a low $TOTCO_3$ level. Similarly, the observed degradation rates of CBZ and ATN were greatly enhanced by 1.4 times from 2 to 0.05 mM $TOTCO_3$ because CBZ and ATN react with $HO^•$ with the same order of magnitude as 1,4-D,[63,67,68] while CBZ and ATN have a lower reactivity with $CO_3^{•-}$ in comparison to SMZ.[69,70] 1,4-D was degraded by $HO^•$ regardless of the $TOTCO_3$ level, while both $HO^•$ and $CO_3^{•-}$ oxidized the other three pharmaceuticals. The sensitivity of $TOTCO_3$ for the four selected compounds toward their oxidative capacity follows the order of 1,4-D > CBZ ≈ATN > SMZ, which is reversely correlated with their reactivities with $CO_3^{•-}$.

Model Prediction of Cumulative $HO^•$ Exposure during $NHCl_2$ Hydrolysis. To further gain a fundamental understanding of $HO^•$ generation initiated by $NHCl_2$ hydrolysis, a mathematical model was established to predict the $HO^•$ exposure during $NHCl_2$ hydrolysis under different solution chemical conditions at pHs between 7 and 12, as shown in eq 1

$$\int_0^t [HO^•]_t \, dt = \alpha\gamma\left(\frac{k_{NHCl_2}k_{ONOO^-}}{k_{NHCl_2} + k_{ONOO^-}}\right)\left(\frac{k_{cont,HO^•}[cont]}{k_{HCO_3^-,HO^•}[HCO_3^-] + k_{cont,HO^•}[cont]}\right)\frac{t}{k_{cont,HO^•}} \quad (1)$$

where $\int_0^t [HO^•]_t dt$ is the cumulative $HO^•$ exposure via $NHCl_2$ hydrolysis-based AOP; α is the $HO^•$ reaction efficiency coefficient, which represents the combined reaction efficiencies of three sequential pathways to generate $HO^•$, including $NHCl_2$ decays into $ONOO^-$ (R1−R6), $ONOO^-$ decomposition to $HO^•$ (R7−R8), and $HO^•$ reaction with chemical of concerns; γ is the NH_2Cl effect factor and is a function of the NH_2Cl-to-$NHCl_2$ molar ratio; k_{NHCl_2} is the *pseudo*-first-order decay rate of $NHCl_2$ at a specific pH, experimentally determined through decomposition experiments conducted at various pH levels by measuring the decrease in $NHCl_2$ concentration over a reaction period of 15 s; k_{ONOO^-} represents the *pseudo*-first-order decay rate of $ONOO^-$ at a specific pH, also experimentally determined through decomposition experiments conducted at various pH levels by measuring the decrease in $ONOO^-$ concentration over a decomposition time of 15 s, t is the reaction time of $NHCl_2$ hydrolysis, which equals to 15 s; $k_{HCO_3^-,HO^•}$ is the second-order rate constant of the reaction between $HO^•$ and HCO_3^- (8.6×10^6 M^{-1} s^{-1}),[40] $k_{cont,HO^•}$ is the second-order rate constant of the reaction between $HO^•$ and a chemical of concern (e.g., with NB, $k_{NB,HO^•} = 4.7 \times 10^9$ M^{-1} s^{-1}),[71] and $[HCO_3^-]$ is the HCO_3^-

https://doi.org/10.1021/acs.est.4c04547
Environ. Sci. Technol. 2024, 58, 13157−13167

concentration at a specific pH; [cont] represents the concentration of chemical of concern (for model fitting, the chemical of concern is NB, which was utilized to quantify the cumulative $HO^{\bullet}$ exposure). The term $\frac{k_{NHCl_2}k_{ONOO^-}}{k_{NHCl_2}+k_{ONOO^-}}$ is a standard kinetic expression to depict coupled sequential reactions, which represents the combined kinetics resulting from sequential reactions of $NHCl_2$ hydrolysis and $ONOO^-$ decomposition for the eventual $HO^{\bullet}$ production. The term $\frac{k_{cont,HO^{\bullet}}[cont]}{k_{HCO_3^-,HO^{\bullet}}[HCO_3^-]+k_{cont,HO^{\bullet}}[cont]}$ is the branching ratio of $HO^{\bullet}$ reacting with the chemical of concern vs reacting with HCO_3^-.

Model fitting using NB decay experimental data at different pHs (Figure 1A) obtained the value of α as 0.25 ± 0.05, which indicated the overall molar efficiency from $NHCl_2$ hydrolysis to $HO^{\bullet}$ production averaged at 25% (details on model fitting are provided in Text S6). Model fitting using NB decay experimental data at different NH_2Cl-to-$NHCl_2$ molar ratios (Figure 3) obtained the value of γ as a function of the NH_2Cl-to-$NHCl_2$ molar ratio. Specifically, the value of γ equals to 1 when the NH_2Cl-to-$NHCl_2$ molar ratio ($\frac{[NH_2Cl]}{[NHCl_2]}$) is zero; $\gamma = 0.23\frac{[NH_2Cl]}{[NHCl_2]} + 1$ when the molar ratio is ≤ 1; $\gamma = -0.3\frac{[NH_2Cl]}{[NHCl_2]} + 1.4$ when the molar ratio is >1 (detailed calculations are provided in Text S6).

The model predicted that NB degradation rates matched very well with the experimentally measured values (Figure S3), indicating the robustness of the mathematical model. The established mathematical model predicted well the experimentally measured cumulative $HO^{\bullet}$ exposure during $NHCl_2$ hydrolysis across all pHs (blue shaded area in Figure 1A), in the presence of NH_2Cl (blue shaded area in Figure 3A,B) and HCO_3^- (blue shaded area in Figure 4A). The model confirmed that the decay of $NHCl_2$ and $ONOO^-$ governs $HO^{\bullet}$ generation during $NHCl_2$ hydrolysis.

In the presence of varying $TOTCO_3$, the cumulative $CO_3^{\bullet-}$ exposure generated via $NHCl_2$ hydrolysis AOP at pH 8.4 is mathematically modeled in eq 2

$$\int_0^t [CO_3^{\bullet-}]_t \, dt = \alpha\gamma\left(\frac{k_{NHCl_2}k_{ONOO^-}}{k_{NHCl_2}+k_{ONOO^-}}\right)\left(\frac{k_{HCO_3^-,HO^{\bullet}}[HCO_3^-]}{k_{HCO_3^-,HO^{\bullet}}[HCO_3^-]+k_{cont,HO^{\bullet}}[cont]}\right)\frac{t}{k_{cont,CO_3^{\bullet-}}} \quad (2)$$

where $\int_0^t [CO_3^{\bullet-}]_t dt$ is the cumulative $CO_3^{\bullet-}$ exposure via $NHCl_2$ hydrolysis-based AOP; α, γ $\left(\frac{k_{NHCl_2}k_{ONOO^-}}{k_{NHCl_2}+k_{ONOO^-}}\right)$, and t are the same as in eq 1; the term $\frac{k_{HCO_3^-,HO^{\bullet}}[HCO_3^-]}{k_{HCO_3^-,HO^{\bullet}}[HCO_3^-]+k_{cont,HO^{\bullet}}[cont]}$ is the branching ratio of $HO^{\bullet}$ reacting with HCO_3^- vs reacting with the chemical of concern; $k_{cont,CO_3^{\bullet-}}$ is the second-order rate constant of the reaction between $CO_3^{\bullet-}$ and a chemical of concern (e.g., with DMA, $k_{DMA,CO_3^{\bullet-}} = 1.8 \times 10^9\ M^{-1}\ s^{-1}$);[72] [cont] represents the concentration of chemical of concern (for model fitting, the chemical of concern is DMA, which was utilized to quantify cumulative $CO_3^{\bullet-}$ exposure). The established mathematical model predicted well the experimentally measured cumulative $CO_3^{\bullet-}$ exposure during $NHCl_2$ hydrolysis across all $TOTCO_3$ levels at the optimal pH of 8.4 (purple-shaded area in Figure 4B).

The optimized model on cumulative $HO^{\bullet}$ and $CO_3^{\bullet-}$ exposure was further utilized to predict the degradation of trace organic contaminants in synthetic RO permeate samples (detailed calculations are provided in Text S5). The model prediction matched well with the experimentally measured *pseudo*-first-order degradation rates (represented by star signs vs bars in Figure 5A). The only exception was a slight underprediction of SMZ degradation, possibly due to an underestimate of the rate constant between $CO_3^{\bullet-}$ and DMA.

$NHCl_2$ Hydrolysis AOP in RO Permeate Condition. The freshly collected RO permeate comprised background NH_2Cl and $NHCl_2$ alongside an oversaturated $TOTCO_3$ level (1.6 mM) with respect to atmospheric CO_2 equilibrium. Conversely, the aerated RO permeate exhibited the same background NH_2Cl and $NHCl_2$ concentrations but a notably reduced $TOTCO_3$ level of 0.2 mM. The $NHCl_2$ hydrolysis AOP demonstrated a significant degradation of trace-level 1,4-D in RO permeate, as depicted in Figure 5B. During standard RO operation, the experimentally observed *pseudo*-first-order degradation rates for 1,4-D were $1.0-1.1 \times 10^{-2}\ s^{-1}$, as determined via direct measurement and the nitrobenzene-based (NB-based) indirect measurement (left panel in Figure 5B). The direct 1,4-D measurement represents the quantification of trace-level 1,4-D degradation occurring during $NHCl_2$ hydrolysis; the NB-based indirect measurement employs NB as a probe for $HO^{\bullet}$, confirming its exposure and subsequent degradation of 1,4-D. The strong agreement of 1,4-D degradation rates between the direct 1,4-D measurement and the NB-based indirect measurement (Figure 5B) further supported the substantial oxidative capacity of $NHCl_2$ hydrolysis AOP under RO permeate conditions. Aeration of fresh RO permeate resulted in a substantial reduction of $TOTCO_3$ by nearly 90% (Table S3), concurrently shifting the pH from a slightly acidic condition toward neutrality. This adjustment brings the system closer to optimal conditions conducive to $NHCl_2$ hydrolysis. Consequently, the *pseudo*-first-order 1,4-D degradation rate was enhanced by approximately 50% to $1.5-1.6 \times 10^{-2}\ s^{-1}$ in aerated RO permeate due to the significant reduction in $TOTCO_3$ (right panel in Figure 5B).

In the RO permeate experimental conditions (Text S8 and Table S4), NH_2Cl and $NHCl_2$ coexist with a NH_2Cl-to-$NHCl_2$ molar ratio of 0.7. As depicted in Figure 3A, cumulative $HO^{\bullet}$ exposure increased with an ascending NH_2Cl-to-$NHCl_2$ molar ratio from 0 to 1. This implies that the oxidative capacity of the $NHCl_2$-driven non-UV AOP is augmented when subjected to realistic NH_2Cl and $NHCl_2$ levels present in the RO permeate. Moreover, prediction from the optimized kinetics model well predicted 1,4-D degradation in the fresh RO permeate and aerated RO permeate from experiments conducted at a potable reuse facility (represented by star signs vs bars in Figure 5B). The consistency between the model-predicted and experimentally observed 1,4-D degradation rates, obtained from experiments employing fresh and aerated RO permeate with varying water chemical parameters (including pH, NH_2Cl, $NHCl_2$, and $TOTCO_3$) from an actual water reuse facility, supported the proposed mathematical model and validated the efficacy of the newly introduced $NHCl_2$ hydrolysis AOP for potable reuse applications. This highlights the applicability of our model to diverse water treatment scenarios, enhancing its potential as a valuable tool for optimizing water reuse processes.

https://doi.org/10.1021/acs.est.4c04547
Environ. Sci. Technol. 2024, 58, 13157−13167

Engineering Implications. The findings of the study provide fundamental mechanistic insights into the $NHCl_2$ hydrolysis-initiated AOP and develop strategies for optimizing RO permeate conditions to maximize treatment efficiency with a significantly reduced energy footprint in water reuse applications (calculation is shown in Text S9). The $NHCl_2$-initiated hydrolysis can be harnessed from the background pre-existing $NHCl_2$ as a complementary non-UV AOP for the rapid degradation of trace organic contaminants in potable reuse. More importantly, this oxidative pathway does not require UV photon energy and efficiently destroys trace organic contaminants in the RO permeate. The trace-level organic contaminants in the RO permeate may differ when the source water shifts. Therefore, water reuse facilities can optimize the extent of aeration and the decarbonation level to maximize removal efficiency, based on the reactivities of $HO^{\bullet}$ and $CO_3^{\bullet-}$ with a particular contaminant, since the radical speciation between $HO^{\bullet}$ and $CO_3^{\bullet-}$ in the RO permeate can be controlled accordingly (detailed calculations are provided in Text S10 and Table S5). In addition, if the target contaminant has high reactivity with both $CO_3^{\bullet-}$ and $HO^{\bullet}$, an aeration step to decarbonate the RO permeate may not be needed, as both radical exposures equally contribute to the degradation of the particular contaminant. The NH_2Cl-to-$NHCl_2$ molar ratio can also be adjusted to maximize radical exposure by controlling the pH and the NH_2Cl disproportionation reaction in the RO feedwater.

Meanwhile, the risk of NDMA formation can be mitigated by implementing a pretreatment step, including membrane-based filtration, to eliminate its precursors. Additionally, employing a post-treatment procedure involving pH adjustment is recommended when utilizing the $NHCl_2$-initiated AOP. Specifically, raising the pH to its maximum level of 8.4 enhances the oxidative capacity of the $NHCl_2$-initiated AOP to its fullest extent. At this optimal pH of 8.4, the formation of NDMA can also be significantly minimized.[21] In essence, while the $NHCl_2$-initiated AOP demonstrates its maximum oxidative capacity, it also proves to be beneficial for NDMA control simultaneously.

■ ASSOCIATED CONTENT

Supporting Information

The Supporting Information is available free of charge at https://pubs.acs.org/doi/10.1021/acs.est.4c04547.

Experimental solution preparation, UV photolysis experiments, mathematical model prediction, radical quantification, and analytical methods (PDF)

■ AUTHOR INFORMATION

Corresponding Author

Haizhou Liu − *Environmental Toxicology Program, University of California, Riverside, California 92521, United States; Department of Chemical and Environmental Engineering, University of California, Riverside, California 92521, United States;* orcid.org/0000-0003-4194-2566; Phone: (951) 827-2076; Email: haizhou@engr.ucr.edu; Fax: (951) 827-5696

Authors

Liang Wu − *Environmental Toxicology Program, University of California, Riverside, California 92521, United States; Department of Chemical and Environmental Engineering, University of California, Riverside, California 92521, United States;* orcid.org/0000-0002-2139-9378

Sitao Liu − *Department of Chemical and Environmental Engineering, University of California, Riverside, California 92521, United States;* orcid.org/0000-0003-1043-9220

Complete contact information is available at: https://pubs.acs.org/10.1021/acs.est.4c04547

Notes

The authors declare no competing financial interest.

■ ACKNOWLEDGMENTS

This study was supported by grants to H.L. from the National Science Foundation (CHE-1808242 and CBET-2131745), the U.S. Bureau of Reclamation (R18AC00114), and the World Water Forum College Grant from the Metropolitan Water District of Southern California. The authors thank Yujie Men and Bosen Jin at the University of California, Riverside for access to an HPLC-HRMS/MS sample analysis, and Ken Ishida at OCWD for assistance in RO permeate experiments and manuscript feedback.

■ REFERENCES

(1) Cao, Z.; Yu, X.; Zheng, Y.; Aghdam, E.; Sun, B.; Song, M.; Wang, A.; Han, J.; Zhang, J. Micropollutant Abatement by the UV/Chloramine Process in Potable Water Reuse: A Review. *J. Hazard. Mater.* **2022**, *424*, No. 127341.

(2) Asano, T.; Levine, A. D. Wastewater Reclamation, Recycling and Reuse: Past, Present, and Future. *Water Sci. Technol.* **1996**, *33* (10−11), 1−14.

(3) Marron, E. L.; Mitch, W. A.; von Gunten, U.; Sedlak, D. L. A Tale of Two Treatments: The Multiple Barrier Approach to Removing Chemical Contaminants during Potable Water Reuse. *Acc. Chem. Res.* **2019**, *52* (3), 615−622.

(4) Asano, T.; Burton, F.; Leverenz, H.; Tsuchihashi, R.; Tchobanoglous, G. *Water Reuse: Issues, Technologies and Applications*; McGraw-Hill: New York, NY, 2007.

(5) Mangalgiri, K. P.; Patton, S.; Wu, L.; Xu, S.; Ishida, K. P.; Liu, H. Optimizing Potable Water Reuse Systems: Chloramines or Hydrogen Peroxide for UV-Based Advanced Oxidation Process? *Environ. Sci. Technol.* **2019**, *53*, 13323−13331.

(6) Ozaki, H.; Li, H. Rejection of Organic Compounds by Ultra-Low Pressure Reverse Osmosis Membrane. *Water Res.* **2002**, *36*, 123−130.

(7) Toor, R.; Mohseni, M. UV-H2O2 Based AOP and Its Integration with Biological Activated Carbon Treatment for DBP Reduction in Drinking Water. *Chemosphere* **2007**, *66* (11), 2087−2095.

(8) Zhao, J.; Peng, J.; Yin, R.; Fan, M.; Yang, X.; Shang, C. Multi-Angle Comparison of UV/Chlorine, UV/Monochloramine, and UV/Chlorine Dioxide Processes for Water Treatment and Reuse. *Water Res.* **2022**, *217*, No. 118414.

(9) Li, W.; Orozco, R.; Camargos, N.; Liu, H. Mechanisms on the Impacts of Alkalinity, PH, and Chloride on Persulfate-Based Groundwater Remediation. *Environ. Sci. Technol.* **2017**, *51* (7), 3948−3959.

(10) Li, W.; Jain, T.; Ishida, K.; Liu, H. A Mechanistic Understanding of the Degradation of Trace Organic Contaminants by UV/Hydrogen Peroxide, UV/Persulfate and UV/Free Chlorine for Water Reuse. *Environ. Sci.: Water Res. Technol.* **2017**, *3* (1), 128−138.

(11) Chuang, Y. H.; Chen, S.; Chinn, C. J.; Mitch, W. A. Comparing the UV/Monochloramine and UV/Free Chlorine Advanced Oxidation Processes (AOPs) to the UV/Hydrogen Peroxide AOP under Scenarios Relevant to Potable Reuse. *Environ. Sci. Technol.* **2017**, *51*, 13859−13868.

(12) Li, W.; Patton, S.; Gleason, J. M.; Mezyk, S. P.; Ishida, K. P.; Liu, H. UV Photolysis of Chloramine and Persulfate for 1,4-Dioxane

Removal in Reverse-Osmosis Permeate for Potable Water Reuse. *Environ. Sci. Technol.* **2018**, *52* (11), 6417−6425.
(13) Patton, S.; Romano, M.; Naddeo, V.; Ishida, K. P.; Liu, H. Photolysis of Mono- and Dichloramines in UV/Hydrogen Peroxide: Effects on 1,4-Dioxane Removal and Relevance in Water Reuse. *Environ. Sci. Technol.* **2018**, *52* (20), 11720−11727.
(14) da Silva, M. K.; Tessaro, I. C.; Wada, K. Investigation of Oxidative Degradation of Polyamide Reverse Osmosis Membranes by Monochloramine Solutions. *J. Membr. Sci.* **2006**, *282*, 375−382.
(15) Xu, P.; Bellona, C.; Drewes, J. E. Fouling of Nanofiltration and Reverse Osmosis Membranes during Municipal Wastewater Reclamation: Membrane Autopsy Results from Pilot-Scale Investigations. *J. Membr. Sci.* **2010**, *353*, 111−121.
(16) Sun, P.; Meng, T.; Wang, Z.; Zhang, R.; Yao, H.; Yang, Y.; Zhao, L. Degradation of Organic Micropollutants in UV/NH2Cl Advanced Oxidation Process. *Environ. Sci. Technol.* **2019**, *53*, 9024−9033.
(17) Wu, Z.; Chen, C.; Zhu, B. Z.; Huang, C. H.; An, T.; Meng, F.; Fang, J. Reactive Nitrogen Species Are Also Involved in the Transformation of Micropollutants by the UV/Monochloramine Process. *Environ. Sci. Technol.* **2019**, *53*, 11142−11152.
(18) Roback, S. L.; Ishida, K. P.; Chuang, Y.-H.; Zhang, Z.; Mitch, W. A.; Plumlee, M. H. Pilot UV-AOP Comparison of UV/Hydrogen Peroxide, UV/Free Chlorine, and UV/Monochloramine for the Removal of N -Nitrosodimethylamine (NDMA) and NDMA Precursors. *ACS ES&T Water* **2021**, *1*, 396−406.
(19) Fehér, P. P.; Purgel, M.; Lengyel, A.; Stirling, A.; Fábián, I. The Mechanism of Monochloramine Disproportionation under Acidic Conditions. *Dalton Trans.* **2019**, *48*, 16713−16721.
(20) Lee, H. J.; Halali, M. A.; Sarathy, S.; de Lannoy, C. F. The Impact of Monochloramines and Dichloramines on Reverse Osmosis Membranes in Wastewater Potable Reuse Process Trains: A Pilot-Scale Study. *Environ. Sci.: Water Res. Technol.* **2020**, *6*, 1336−1346.
(21) McCurry, D. L.; Ishida, K. P.; Oelker, G. L.; Mitch, W. A. Reverse Osmosis Shifts Chloramine Speciation Causing Re-Formation of NDMA during Potable Reuse of Wastewater. *Environ. Sci. Technol.* **2017**, *51*, 8589−8596.
(22) Patton, S. D.; Dodd, M. C.; Liu, H. Degradation of 1,4-Dioxane by Reactive Species Generated during Breakpoint Chlorination: Proposed Mechanisms and Implications for Water Treatment and Reuse. *J. Hazard. Mater. Lett.* **2022**, *3*, No. 100054.
(23) Wu, L.; Patton, S. D.; Liu, H. Mechanisms of Oxidative Removal of 1, 4-Dioxane via Free Chlorine Rapidly Mixing into Monochloramine: Implications on Water Treatment and Reuse. *J. Hazard. Mater.* **2022**, *440*, No. 129760.
(24) Selbes, M.; Beita-Sandí, W.; Kim, D.; Karanfil, T. The Role of Chloramine Species in NDMA Formation. *Water Res.* **2018**, *140*, 100−109.
(25) Pham, H. T.; Wahman, D. G.; Fairey, J. L. Closing Dichloramine Decomposition Nitrogen and Oxygen Mass Balances: Relative Importance of End-Products from the Reactive Nitrogen Species Pathway. *Environ. Sci. Technol.* **2024**, *58* (4), 2048−2057.
(26) Pham, H. T.; Wahman, D. G.; Fairey, J. L. Updated Reaction Pathway for Dichloramine Decomposition: Formation of Reactive Nitrogen Species and N-Nitrosodimethylamine. *Environ. Sci. Technol.* **2021**, *55* (3), 1740−1749.
(27) Schreiber, I. M.; Mitch, W. A. Enhanced Nitrogenous Disinfection Byproduct Formation near the Breakpoint: Implications for Nitrification Control. *Environ. Sci. Technol.* **2007**, *41*, 7039−7046.
(28) Merényi, G.; Lind, J. Free Radical Formation in the Peroxynitrous Acid (ONOOH)/Peroxynitrite (ONOO-) System. *Chem. Res. Toxicol.* **1998**, *11*, 245−246.
(29) Sgroi, M.; Vagliasindi, F. G. A.; Snyder, S. A.; Roccaro, P. N-Nitrosodimethylamine (NDMA) and Its Precursors in Water and Wastewater: A Review on Formation and Removal. *Chemosphere* **2018**, *191*, 685−703.
(30) Landsman, N. A.; Swancutt, K. L.; Bradford, C. N.; Cox, C. R.; Kiddle, J. J.; Mezyk, S. P. Free Radical Chemistry of Advanced Oxidation Process Removal of Nitrosamines in Water. *Environ. Sci. Technol.* **2007**, *41* (16), 5818−5823.
(31) Valentine, R. L.; Jafvert, C. T. Reaction Scheme for the Chlorination of Ammoniacal Water. *Environ. Sci. Technol.* **1992**, *26* (3), 577−586.
(32) Benjamin, M. M. *Water Chemistry*, 2nd ed.; Waveland Press, Inc: Long Grove, IL, 2015.
(33) Vikesland, P. J.; Ozekin, K.; Valentine, R. L. Monochloramine Decay in Model and Distribution System Waters. *Water Res.* **2001**, *35* (7), 1766−1776.
(34) Hossain, S.; Chow, C. W. K.; Cook, D.; Sawade, E.; Hewa, G. A. Review of Chloramine Decay Models in Drinking Water System. *Environ. Sci.: Water Res. Technol.* **2022**, *8*, 926−948.
(35) Khan, A. U.; Kovacic, D.; Kolbanovskiy, A.; Desai, M.; Frenkel, K.; Geacintov, N. E. The Decomposition of Peroxynitrite to Nitroxyl Anion (NO-) and Singlet Oxygen in Aqueous Solution. *Proc. Natl. Acad. Sci. U. S. A.* **2000**, *97* (7), 2984−2989.
(36) Coddington, J. W.; Hurst, J. K.; Lymar, S. V. Hydroxyl Radical Formation during Peroxynitrous Acid Decomposition. *J. Am. Chem. Soc.* **1999**, *121* (11), 2438−2443.
(37) Shafirovich, V.; Lymar, S. V. Nitroxyl and Its Anion in Aqueous Solutions: Spin States, Protic Equilibria, and Reactivities toward Oxygen and Nitric Oxide. *Proc. Natl. Acad. Sci. U.S.A.* **2002**, *99* (11), 7340−7345.
(38) Buxton, G. V.; Elliot, A. J. Rate Constant for Reaction of Hydroxyl Radicals with Bicarbonate Ions. *Int. J. Radiat. Appl. Instrum., Part C* **1986**, *27* (3), 241−243.
(39) Goldstein, S.; Lind, J.; Merényi, G. Chemistry of Peroxynitrites as Compared to Peroxynitrates. *Chem. Rev.* **2005**, *105*, 2457−2470.
(40) Buxton, G. V.; Greenstock, C. L.; Helman, W. P.; Ross, A. B. Critical Review of Rate Constants for Reactions of Hydrated Electrons, Hydrogen Atoms and Hydroxyl Radicals (·OH/·O− in Aqueous Solution. *J. Phys. Chem. Ref. Data* **1988**, *17*, 513−886.
(41) Li, W.; Xu, E.; Schlenk, D.; Liu, H. Cyto- and Geno-Toxicity of 1,4-Dioxane and Its Transformation Products during Ultraviolet-Driven Advanced Oxidation Processes. *Environ. Sci.: Water Res. Technol.* **2018**, *4* (9), 1213−1218.
(42) Zenker, M. J.; Borden, R. C.; Barlaz, M. A. Occurrence and Treatment of 1,4-Dioxane in Aqueous Environments. *Environ. Eng. Sci.* **2003**, *20* (5), 423−432.
(43) Roback, S. L.; Ferrer, I.; Thurman, E. M.; Ishida, K. P.; Plumlee, M. H.; Poustie, A.; Westerhoff, P.; Hanigan, D. Non-Target Mass Spectrometry Analysis of NDMA Precursors in Advanced Treatment for Potable Reuse. *Environ. Sci.: Water Res. Technol.* **2018**, *4* (12), 1944−1955.
(44) Alturki, A. A.; Tadkaew, N.; McDonald, J. A.; Khan, S. J.; Price, W. E.; Nghiem, L. D. Combining MBR and NF/RO Membrane Filtration for the Removal of Trace Organics in Indirect Potable Water Reuse Applications. *J. Membr. Sci.* **2010**, *365* (1−2), 206−215.
(45) Crook, J.; Bull, R.; Collins, H. F.; Cotruvo, J. A.; Jakubowski, W. *Examining the Criteria for Direct Potable Reuse: Recommendations of an NWRI Independent Advisory Panel*; National Water Research Institute: Fountain Valley, CA, 2013.
(46) Hughes, M. N.; Nicklin, H. G. The Chemistry of Pernitrites. Part I. Kinetics of Decomposition of Pernitrous Acid. *J. Chem. Soc. A* **1968**, *450*, 450−452.
(47) Canonica, S.; Meunier, L.; von Gunten, U. Phototransformation of Selected Pharmaceuticals during UV Treatment of Drinking Water. *Water Res.* **2008**, *42* (1−2), 121−128.
(48) Clesceri, L. S.; Greenberg, S. E.; Trussell, R. R. *Standard Methods for the Examination of Water and Wastewater*, 17th ed.; American Public Health Association: Washington DC, 1989.
(49) Larson, T. E.; Henley, L. Determination of Low Alkalinity or Acidity in Water. *Anal. Chem.* **1955**, *27*, 851−852, DOI: 10.1021/ac60101a051.
(50) Sellers, R. M. Spectrophotometric Determination of Hydrogen Peroxide Using Potassium Titanium(IV) Oxalate. *Analyst* **1980**, *105* (1255), 950−954.

(51) Liang, C.; Huang, C. F.; Mohanty, N.; Kurakalva, R. M. A Rapid Spectrophotometric Determination of Persulfate Anion in ISCO. *Chemosphere* **2008**, *73* (9), 1540−1543.
(52) Huang, J.; Mabury, S. A. Steady-State Concentrations of Carbonate Radicals in Field Waters. *Environ. Toxicol. Chem.* **2000**, *19* (9), 2181−2188.
(53) Neta, P.; Huie, R. E.; Ross, A. B. Rate Constants for Reactions of Inorganic Radicals in Aqueous Solution. *J. Phys. Chem. Ref. Data* **1988**, *17* (3), 1027−1284.
(54) Saunier, B. M.; Selleck, R. E. Kinetics of Breakpoint Chlorination in Continuous Flow Systems. *J. AWWA* **1979**, *71* (3), 164−172.
(55) Wahman, D. G.; Speitel, G. E.; Machavaram, M. V. A Proposed Abiotic Reaction Scheme for Hydroxylamine and Monochloramine under Chloramination Relevant Drinking Water Conditions. *Water Res.* **2014**, *60*, 218−227.
(56) Johnson, H. D.; Cooper, W. J.; Mezyk, S. P.; Bartels, D. M. Free Radical Reactions of Monochloramine and Hydroxylamine in Aqueous Solution. *Radiat. Phys. Chem.* **2002**, *65* (4−5), 317−326.
(57) Shafirovich, V.; Lymar, S. V. Spin-Forbidden Deprotonation of Aqueous Nitroxyl (HNO). *J. Am. Chem. Soc.* **2003**, *125* (21), 6547−6552.
(58) Goldstein, S.; Rabani, J. Mechanism of Nitrite Formation by Nitrate Photolysis in Aqueous Solutions: The Role of Peroxynitrite, Nitrogen Dioxide, and Hydroxyl Radical. *J. Am. Chem. Soc.* **2007**, *129* (34), 10597−10601.
(59) Jayson, G. G.; Parsons, B. J.; Swallow, A. J. Some Simple, Highly Reactive, Inorganic Chlorne Derivatives in Aqueous Solution. *J. Chem. Soc., Faraday Trans. 1* **1973**, *69*, 1597−1607.
(60) Anbar, M.; Yagil, G. The Hydrolysis of Chloramine in Alkaline Solution. *J. Am. Chem. Soc.* **1962**, *84* (10), 1790−1796.
(61) Giles, B. J. The Oxidation of Hydroxylamine by Hypohalites and Other Halogen-Containing Species. Ph.D. Thesis. Purdue University: West Lafayette, IN, 1999.
(62) Lymar, S. V.; Hurst, J. K. CO2-Catalyzed One-Electron Oxidations by Peroxynitrite: Properties of the Reactive Intermediate. *Inorg. Chem.* **1998**, *37* (2), 294−301.
(63) Borowska, E.; Felis, E.; Miksch, K. Degradation of Sulfamethoxazole Using UV and UV/H2O2 Processes. *J. Adv. Oxid. Technol.* **2015**, *18* (1), 69−77.
(64) Wojnárovits, L.; Tóth, T.; Takács, E. Rate Constants of Carbonate Radical Anion Reactions with Molecules of Environmental Interest in Aqueous Solution: A Review. *Sci. Total Environ.* **2020**, *717*, No. 137219.
(65) Eibenberger, J. *Pulse Radiolytic Investigations Concerning the Formation and the Oxidation of Organic Radicals in Aqueous Solutions*; Vienna University, 1980.
(66) Cope, V. W.; Huffman, M. Z.; Chen, S. N. Reactivity of the Carbonate Radical toward Metal Complexes in Aqueous Solution. *J. Phys. Chem. A* **1978**, *82* (25), 2665−2669.
(67) Ali, F.; Khan, J. A.; Shah, N. S.; Sayed, M.; Khan, H. M. Carbamazepine Degradation by UV and UV-Assisted AOPs: Kinetics, Mechanism and Toxicity Investigations. *Process Saf. Environ. Prot.* **2018**, *117*, 307−314.
(68) Benner, J.; Salhi, E.; Ternes, T.; von Gunten, U. Ozonation of Reverse Osmosis Concentrate: Kinetics and Efficiency of Beta Blocker Oxidation. *Water Res.* **2008**, *42* (12), 3003−3012.
(69) Wols, B. A.; Harmsen, D. J. H.; Beerendonk, E. F.; Hofman-Caris, C. H. M. Predicting Pharmaceutical Degradation by UV (LP)/H2O2 Processes: A Kinetic Model. *Chem. Eng. J.* **2014**, *255*, 334−343.
(70) Jasper, J. T.; Sedlak, D. L. Phototransformation of Wastewater-Derived Trace Organic Contaminants in Open-Water Unit Process Treatment Wetlands. *Environ. Sci. Technol.* **2013**, *47*, 10781−10790.
(71) Asmus, K. D.; Cercek, B.; Ebert, M.; Henglein, A.; Wigger, A. Pulse Radiolysis of Nitrobenzene Solutions. *Trans. Faraday Soc.* **1967**, *63* (5), 2435−2441.
(72) Ross, A. B.; Neta, P. *Rate Constants for Reactions of Inorganic Radicals in Aqueous Solution*; National Bureau of Standards, 1979; 1−55.

https://doi.org/10.1021/acs.est.4c04547
Environ. Sci. Technol. 2024, 58, 13157−13167